ELSEVIER

Chemical Physics 239 (1998) 393–407

Chemical Physics

Infrared photodissociation spectra of isomeric $SiOH^+–Ar_n$ $(n = 1–10)$ complexes

Rouslan V. Olkhov, Sergey A. Nizkorodov [1], Otto Dopfer *

Institut für Physikalische Chemie, Universität Basel, Klingelbergstrasse 80, CH-4056, Basel, Switzerland

Received 20 April 1998

Abstract

Infrared photodissociation spectra of mass-selected $SiOH^+–Ar_n$ complexes $(n = 1–10)$ have been recorded in the vicinity of the OH stretch (ν_1) vibration of $SiOH^+$. The $SiOH^+–Ar$ dimer has also been investigated by ab initio calculations at the MP2 level and two stable isomers have been found. The linear proton-bound global minimum $(D_e = 1117\ cm^{-1})$ and the less stable T-shaped silicon-bound geometry $(D_e = 938\ cm^{-1})$ are separated by an isomerization barrier of $\sim 500\ cm^{-1}$. Three rotationally resolved bands observed in the dimer spectrum are assigned to the ν_1 fundamental $(3444.9\ cm^{-1})$ and the $\nu_1 + \nu_s$ $(3554.6\ cm^{-1})$ and $\nu_1 + 2\nu_b$ $(3581.5\ cm^{-1})$ combination bands of the linear isomer, whereas a weak unresolved band centered at $3673\ cm^{-1}$ is attributed to the ν_1 fundamental of the T-shaped isomer. The assignments are based on the rotational analysis, vibrational frequencies and comparison with the ab initio results. Systematic ν_1 vibrational band shifts observed in the spectra of larger clusters have allowed to monitor the cluster growth and identify coexisting isomers.

1. Introduction

Weak intermolecular interactions are responsible for many fundamental physical, chemical and biological properties and processes, like solvation, macromolecule folding and recognition, physisorption, condensation, etc. [1–3]. To understand these phenomena from the microscopic point of view, a detailed knowledge of the interaction potential acting between the participating molecules is required. High-resolution spectroscopic techniques have proven to be useful tools in characterizing the potential energy surfaces of small weakly-bound aggregates [4–6]. Due to fruitful interplay between experiment and ab initio and/or semi-empirical theories, for a few small neutral dimers and trimers accurate surfaces are now available that can reproduce the experimental data to high precision [5,7,8].

In contrast to neutral complexes, high-resolution spectroscopic data on ionic molecular clusters are still rare, mainly because of the difficulties associated with the production of large number densities of these species [9]. High selectivity and sensitivity of predissociation spectroscopy combined with mass spectrometric techniques can overcome this problem [10] and it is mostly by this approach that high-resolution spectra have been recorded for charged complexes in the microwave [11], mid-infrared [12,13] and visible/ultraviolet [14,15] parts of the electromagnetic spectrum.

* Corresponding author. E-mail: dopfer@ubaclu.unibas.ch

[1] Present address: JILA, University of Colorado, Boulder, CO 80309-0440, USA.

0301-0104/98/$ - see front matter
PII: S0301-0104(98)00253-5

In our laboratory the structure and dynamics of a series of proton-bound dimers of the form AH^+–B have systematically been characterized by their mid-infrared photofragmentation spectra. The interest in such species arises partly from the fact that they are intermediates in proton transfer reactions [16–19]. For all of the complexes studied so far the proton affinity (PA) of the base A (e.g., CO [20–24], N_2 [25–28], NH_3 [29–31], O_2 [32], O [33]) is considerably larger than that of the base B, which is either a rare gas atom (Rg = He, Ne, or Ar) or molecular hydrogen. These complexes can therefore be viewed to a first approximation as an AH^+ molecule weakly distorted by the ligand B. The proton is slightly attracted by the moiety B leading to a moderate destabilization of the AH^+ bond. The extent of the proton transfer, the accompanying reduction in the A–H stretching frequency, and the complex's dissociation energy are correlated with the difference in the proton affinities of the two involved bases [34]. For example, for the Rg–HCO^+ series (Rg = He, Ne, Ar) a linear correlation between the rare gas atom's proton affinity and the red shift of the C–H stretching vibration has been observed [21].

As a general rule, proton-bound dimers AH^+–B prefer configurations where the proton is most effectively shared between the two bonded bases [9,12,13]. For example, the complexes Rg–HCO^+ (Rg = He, Ne, Ar) [20–22,35], Rg–HN_2^+ (Rg = He, Ne, Ar) [25–27,36,37] and Rg–HO^+ (Rg = He, Ne) [33] are linear, while H_2–HCO^+ and H_2–HN_2^+ are found to be T-shaped [23,24,28]. Though the NH_4^+–Rg complexes (Rg = He, Ne and Ar) do not possess sufficient angular rigidity to rigorously specify their structure in customary terms of bond lengths and angles, the Rg ligand prefers the vertex-bound site [29–31]. As SiO is isovalent to CO and N_2, the structure of the complex composed of $SiOH^+$ and Ar is anticipated to be linear with the rare gas atom attached to the proton end of $SiOH^+$. Moreover, as the PA of SiO (792 kJ/mol) exceeds those of CO (594 kJ/mol) and N_2 (495 kJ/mol), the intermolecular bond in the $SiOH^+$–Ar complex is expected to be weaker than in either Ar–HCO^+ ($D_0 \approx 1600$ cm^{-1} [38]) or Ar–HN_2^+ ($D_0 = 2781.5 \pm 1.5$ cm^{-1} [27]).

Not all ionic complexes of the form AH^+–B belong to the proton-bound class. For example, the CH_3^+–Ar dimer can be best characterized as a charge-transfer complex, where the Ar atom prefers the π-bound site to the proton-bound one [39]. The bond formation is accompanied by electron density transfer from the Ar atom to the vacant electrophilic $2p_z$ orbital on the C atom [39,40]. The lowest unoccupied molecular orbital (LUMO) in $SiOH^+$ correlates to the empty 3p orbital of the free Si atom. As the Si atom in $SiOH^+$ bears significant positive charge density, a T-shaped Si-bound geometry of the Ar–$SiOH^+$ complex is also conceivable where the Ar atom may donate some charge into the LUMO of $SiOH^+$. In fact, the experimental data and ab initio calculations presented below suggest that both proton-bound and T-shaped isomers exist and have comparable binding energies.

In addition to the $SiOH^+$–Ar dimer, spectra of larger $SiOH^+$–Ar_n clusters containing up to 10 argon atoms have also been recorded. In a previous study of the related HCO^+–Ar_n series ($n = 1$–13), cluster structures were inferred from the Ar atom induced shifts in the ν_1 transition frequency (CH stretch), combination band positions, and photofragmentation yields [22]. The data are in accord with cluster geometries where a linear proton-bound Ar–HCO^+ ion core is surrounded by less strongly bound Ar atoms. The ligands first fill two five-membered solvation rings around the linear dimer core, with the first solvation shell being completed by the attachment of the twelfth Ar atom at the oxygen end (leading to an icosahedral structure with HCO^+ in the center). A similar cluster growth mechanism has been invoked for He_n–HN_2^+ ($n = 1$–2 [36]), Ne_n–HCO^+ ($n = 1$–2 [21]), and Ne_n–HN_2^+ ($n = 1$–5 [26]) though the lower binding energies in these complexes have limited the studies to smaller cluster sizes. Thus, the spectra of $SiOH^+$–Ar_n with n up to 10 provide a more direct and complete comparison with the HCO^+–Ar_n series.

Protonated silicon monoxide, which serves as the infrared (IR) chromophore in the $SiOH^+$–Ar_n complexes, is considered as an important intermediate in ionospheric and interstellar chemistry of Si-containing species [41,42]. The potential energy surface of $SiOH^+$ has been characterized by numerous theoretical studies at various levels of theory providing detailed information about the structural, dynamical and energetical properties of its various isomeric

forms [43–48]. In contrast to the isovalent CO molecule, for which the PA for protonation at the C site (594 kJ/mol [18]) is larger than on the O end (456 kJ/mol [49]), all calculations predict the opposite situation for SiO. Linear $SiOH^+$ is calculated [48] to be ~ 270 kJ/mol more stable than linear $HSiO^+$ and both minima are separated by a large isomerization barrier (114 kJ/mol). The PA of SiO for protonation on the O side has experimentally been determined as 792 ± 11 kJ/mol [50].

In contrast to the situation on the theoretical side, experimental spectroscopic data for $SiOH^+$ are scarce [51,52]. Probably due to the small dipole moment, no microwave spectrum of $SiOH^+$ has been reported [48]. The measured fundamental frequencies for the OH stretch ($\nu_1 = 3662$ cm^{-1}) and SiO stretch ($\nu_3 = 1127$ cm^{-1}) vibrations of the $^1\Sigma^+$ electronic ground state are in good agreement with the theoretical predictions [51,52]. Experiments on isotopic species provided interatomic distances of $r_{O-H} = 0.940$ Å and $r_{Si-O} = 1.537$ Å [51]. The frequency of the bending vibration, calculated as $\nu_2 = 373 \pm 10$ cm^{-1}, has not yet been measured [46]. In contrast to the fundamentals which all have large IR transition strengths, overtone and combination bands are predicted to be extremely weak [46,48].

Several complexes of the type $SiOH^+$–X with closed-shell molecules X have been identified in mass spectrometric studies [50,53]. Some of them correspond to collisionally stabilized intermediates of chemical reactions involving $SiOH^+$ and X. However, no spectral data appear to exist on $SiOH^+$–X complexes and the present study of $SiOH^+$–Ar provides the first spectroscopic information about their structure and stability.

As the weak intermolecular bonds in the $SiOH^+$–Ar_n complexes cause only small effects on the free monomer vibrations, the notation employed for the cluster vibrations refers to the normal modes of the $SiOH^+$ chromophore (ν_{1-3}). The intermolecular stretch and bend vibrations of the $SiOH^+$–Ar dimer are designated ν_s and ν_b, respectively.

2. Experimental

Mid-infrared predissociation spectra of mass-selected $SiOH^+$–Ar_n complexes ranging from $n = 1$ to 10 were measured in a tandem mass spectrometer apparatus described in detail previously [15,22].

The cluster ions were produced by expanding a suitable gas mixture through a pulsed valve. Close to the nozzle orifice the supersonic expansion was crossed by 100 eV electron beams emitted from two heated tungsten filaments. Electron impact ionization processes were followed by a variety of ion–molecule and clustering reactions to form weakly-bound $SiOH^+$–Ar_n complexes. The gas mixture employed for the dimer ($n = 1$) contained SiH_4, O_2, He, and Ar in a ratio of 1:24:100:800 at a stagnation pressure of 8 bar. To increase the ion currents of the larger complexes ($n = 2$–10) the relative proportion of Ar in the mixture was gradually increased up to 2000 for $n = 10$. Fig. 1 displays parts of a mass spectrum taken under typical experimental conditions showing the Ar_n^+, H^+–Ar_n, O_{2m}^+–Ar_n, $SiOH^+$–Ar_n, $SiOH^+$–O_2–Ar_n and SiH_m^+–Ar_n cluster series as the dominant species.

After passing through a skimmer, the $SiOH^+$–Ar_n parent complexes were selected from the variety of cluster ions present in the beam by a quadrupole mass spectrometer (QMS). Subsequently, the parent ion beam was injected into an octopole ion guide

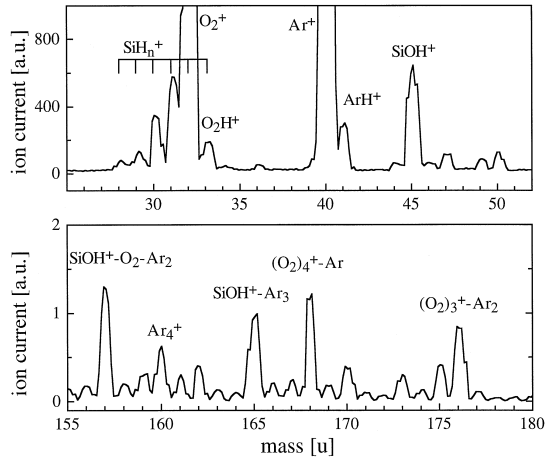

Fig. 1. Representative mass spectra of the ions produced in the cluster ion source in the mass range of the $SiOH^+$ monomer (top) and the $SiOH^+$–Ar_3 complex (bottom, vertically expanded by a factor 500). Species including O_2 and SiH_4 interfere with each other as both molecules have the same mass (32 u); however, mass spectra taken without SiH_4 show that the contributions arising from O_2 dominate.

where it was exposed to tunable infrared radiation. Resonant excitation into predissociating rovibrational levels induced the clusters' dissociation into $SiOH^+$–Ar_m product ions and $(n-m)$ Ar atoms. The second QMS transmitted only the desired fragment ions, which were measured by a Daly ion detector [54]. Predissociation spectra were obtained by monitoring the dependence of the fragment ion yield on the excitation frequency. In cases where more than one significant fragment channel was observed, spectra were recorded for each of them. To separate the contribution of fragment ions produced by laser-induced dissociation from the background signal, which mainly arose from metastable decay of hot parent complexes in the octopole region, the ion source was triggered at twice the laser frequency, and the signal acquired with the laser off was subtracted from that with the laser on.

Infrared laser radiation was produced by a Nd:YAG laser pumped optical parametric oscillator (OPO) system characterized by a 0.02 cm^{-1} bandwidth, 2500–6900 cm^{-1} tuning range, 0.5–5 mJ/pulse intensity, 5 ns pulse width, and a repetition rate of 20 Hz. The predissociation spectra were calibrated against etalon transmission fringes of the OPO oscillator and optoacoustic spectra of the reference gases NH_3 and $H_2O/D_2O/HDO$ recorded using the idler and signal outputs of the OPO system [55]. The spectra were linearly normalized for laser power and corrected for the Doppler shift arising from the kinetic energy of the ions in the octopole (3 ± 1 eV). The absolute accuracy of rotational line positions is limited to ~ 0.01 cm^{-1}, due to a combination of the laser bandwidth and the uncertainty in the ion kinetic energy.

3. Ab initio calculations

Ab initio calculations using the Gaussian 94 program package [56] were carried out to assist the interpretation of the experimental results. The $SiOH^+$ monomer and the $SiOH^+$–Ar dimer have been investigated at the MP2 level of theory, utilizing a basis set composed of an Ahlrichs VTZ basis for the core electrons augmented with diffuse and polarization functions taken from the aug-cc-pVTZ basis set (abbreviated VTZ$*$ in the tables) [57]. The contraction scheme can be described as Si(13s, 10p, 3d, 2f) → [8s, 6p, 3d, 2f], O(11s, 7p, 3d, 2f) → [7s, 4p, 3d, 2f], H(6s, 3p, 2d) → [4s, 3p, 2d] and Ar(13s, 10p, 3d, 2f) → [8s, 6p, 3d, 2f]. All coordinates were allowed to relax during the search for stationary points. For the determination of intermolecular binding energies (D_e) of the dimer the calculated interaction energies were corrected for the basis set superposition error [58] and the relaxation energy arising from the changes in the monomer geometry upon formation of the complex [59]. The results of the calculations are summarized in Fig. 2 and Tables 1 and 2. Computed harmonic frequencies were scaled by a factor 0.961 to match the calculated and experimental values for the ν_1 frequency of $SiOH^+$.

In agreement with previous theoretical studies, the linear oxygen-protonated structure was found to be the global minimum for the $SiOH^+$ monomer. Table 1 compares the geometry and fundamental frequencies calculated at the MP2 level with those obtained at the higher CCSD(T) level [48] and available experimental data [51,52]. Satisfying agreement is obtained for the geometrical data and the two stretching vibrations, whereas the frequency of the floppy bending motion appears to depend significantly on the level of theory [44,46,48].

Several minima structures were found on the intermolecular potential energy surface of the $SiOH^+$–Ar complex. The global minimum corresponds to the linear proton-bound geometry (structure I in Fig. 2) with a binding energy $D_e = 1117$ cm^{-1} and an inter-

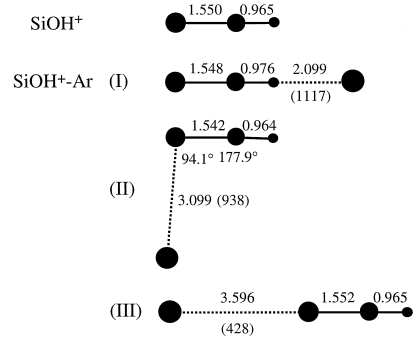

Fig. 2. Ab initio calculated geometries (distances in Å) of the $SiOH^+$ monomer and three isomers on the $SiOH^+$–Ar dimer: linear proton-bound global minimum (I), T-shaped local minimum (II), and anti-linear structure (III). Binding energies D_e in cm^{-1} are given in brackets.

Table 1
Calculated r_e bond lengths (in Å) and harmonic and scaled frequencies (ω_i and ν_i, in cm^{-1}) of linear $SiOH^+$ compared to experimental data (ν_i and r_0)

Method/basis	r_{Si-O}	r_{O-H}	$\omega_1/\nu_1\sigma$	$\omega_2/\nu_2\ \pi$	$\omega_3/\nu_3\ \sigma$
MP2/VTZ*	1.5500	0.9650	3811/3662 (596)	424/407 (472)	1127/1083 (132)
CCSD(T)/TZ2P(f,d) + diff[a]	1.5422	0.9631	3856/–(565)	339/–(477)	1128/–(128)
exp.[b]	1.537	0.940	–/3662.36		–/1127.01

Infrared intensities (in km/mol) are given in brackets.
[a]Ref. [48].
[b]Refs. [51,52].

molecular separation $r_{H-Ar} = 2.099$ Å. As expected, the O–H bond is noticeably prolonged upon formation of the complex ($\Delta r_{O-H} = 0.011$ Å), and consequently the ν_1 frequency is strongly red-shifted ($\Delta\nu_1 = -246\ cm^{-1}$) from the monomer value. In contrast, the Si–O bond is only slightly shortened ($\Delta r_{Si-O} = -0.002$ Å) leading to a small increase in the ν_3 frequency ($\Delta\nu_1 = 14\ cm^{-1}$). The bending frequency (ν_2) increases substantially (by a factor of 1.6) due to the additional angular constraints arising from the formation of the intermolecular bond.

The second minimum localized on the dimer surface can be described as a 'T-shaped' configuration (structure II in Fig. 2). It is characterized by a well depth $D_e = 938\ cm^{-1}$, an intermolecular separation $r_{Ar-Si} = 3.099$ Å and a bond angle ∠Ar–Si–O = 94.1°. Though the intermolecular interaction strength in the T-shaped isomer is comparable with that in the proton-bound one, the geometry and frequencies of the $SiOH^+$ core are less affected upon complex formation. The energy of the transition state between both isomers has been estimated as $D_e \approx 450\ cm^{-1}$, giving rise to a barrier of $\sim 500\ cm^{-1}$ for the transition from the T-shaped to the global minimum structure.

The linear silicon-bound dimer geometry (structure III in Fig. 2) is significantly higher in energy than the T-shaped configuration, as is evidenced by the longer and weaker intermolecular bond ($D_e = 428\ cm^{-1}$, $r_{Ar-Si} = 3.596$ Å). Consequently, the monomer properties are only slightly affected by Ar complexation. According to the frequency calculation at the

Table 2
Calculated structures (in Å, deg), binding energies D_e and scaled harmonic frequencies (in cm^{-1}) of three isomers of $SiOH^+$–Ar (Fig. 2) at the MP2/VTZ* level

Isomer	r_{Si-O}	r_{O-H}	r_{H-Ar}/r_{Si-Ar}	∠Si–O–H	∠Ar–Si–O	D_e
I	1.5477	0.9764	2.0990/–	180.0	0.0	1117
II	1.5423	0.9639	–/3.0994	177.9	94.1	938
III	1.5518	0.9649	–/3.5962	180.0	180.0	428

Isomer	ν_1	ν_2	ν_3	ν_s	ν_b
I ($C_{\infty v}$)	3416 (1826/σ)	636 (155/π)	1097 (92/σ)	116 (26/σ)	84 (6/π)
II (C_S)	3678 (575/a′)	374 (246/a′) 404 (225/a″)	1076 (128/a′)	62 (12/a′)	100 (19/a′)
III ($C_{\infty v}$)	3665 (610/σ)	419 (462/π)	1077 (158/σ)	55 (15/σ)	18 (2/π)

Infrared intensities (in km/mol) and symmetries of the fundamentals are given in brackets.

MP2 level, this 'anti-linear' dimer configuration corresponds to a local minimum. However, the barrier along the path towards the T-shaped local minimum is very small (< 10 cm^{-1}) and the anti-linear isomer becomes a transition state at the HF level. Thus, in contrast to the deep proton-bound and T-shaped minima which are separated by large barriers, it is not clear whether the anti-linear structure is a very shallow minimum or in fact a transition state between two T-shaped configurations.

The existence of several stable isomers on the $SiOH^+$–Ar dimer potential energy surface might at first glance be surprising, because for the related N_2H^+–Ar and OCH^+–Ar complexes only a single minimum corresponding to the proton-bound linear geometry (structure I) was predicted [60–62] and experimentally found [22,27,35,37]. However, the charge distributions in the three considered chromophore ions are quite different. Whereas in N_2H^+ the positive charge is roughly equally distributed between the three atoms [28], it is almost equally shared between the C and H atoms in HCO^+ [63]. As the proton is small, these charge distributions strongly favor linear proton-bound configurations for the complexes of these two ions with Ar. In contrast, in $SiOH^+$ the charge is mainly localized on the Si atom. Thus, cluster geometries with the Ar atom close to the Si atom gain in stability due to enhanced inductive interactions. The T-shaped structure may be additionally stabilized by a partial charge transfer from Ar to Si. Both effects lead to the existence of the T-shaped minimum, but they are not strong enough to make this structure lower in energy than the linear proton-bound global minimum.

4. Experimental results and discussion

4.1. $SiOH^+$–Ar dimer

Fig. 3 presents the mid-infrared photodissociation spectrum of the $SiOH^+$–Ar complex (85 u) recorded

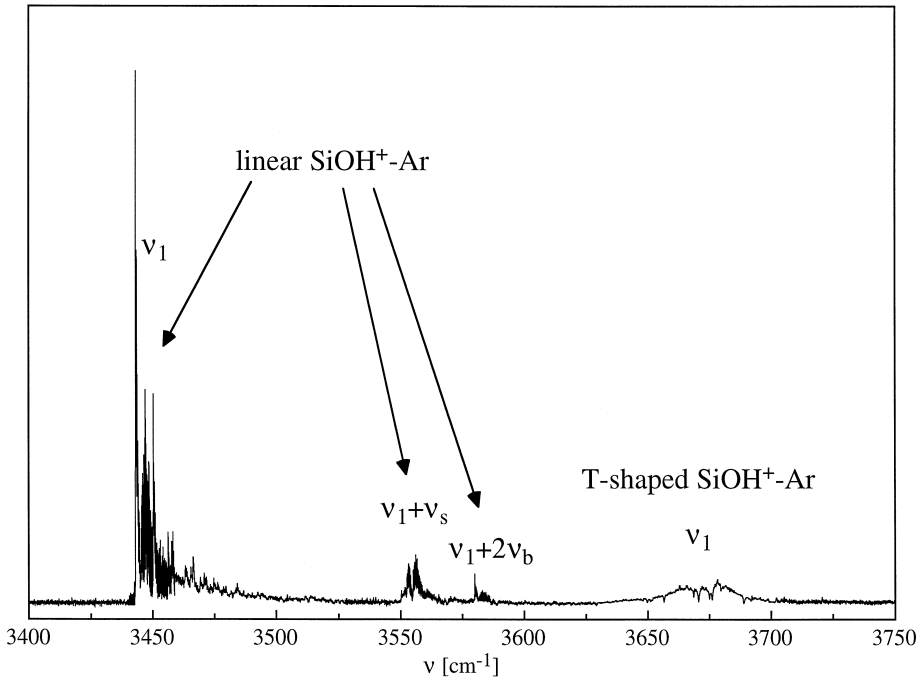

Fig. 3. Infrared predissociation spectrum of the $SiOH^+$–Ar dimer recorded in the $SiOH^+$ fragment channel. As this overview spectrum is composed of several scans, the relative intensities of widely spaced bands are only approximate. Three bands on the left are assigned to the proton-bound linear structure while the broad feature is attributed to the less stable T-shaped isomer. Dips in the contour of the latter band are due to strong atmospheric water absorptions in this spectral range.

in the $SiOH^+$ fragment channel (45 u). Four stronger bands are readily observed in the range 3100–3850 cm^{-1}. Three transitions centered at 3444.9, 3554.6, and 3581.5 cm^{-1} display rotationally resolved structure (Fig. 4), and their Σ–Σ type character indicates that they arise from a (quasi-)linear species. The fourth band at 3673 ± 5 cm^{-1} is significantly broader and not resolved.

Double mass selection in the present experiment reliably defines the composition of the absorbing cluster ion. However, it does not provide an assignment of the observed bands to possible structural isomers of the parent ion. From the preceding discussion, it is clear that both proton-bound and T-shaped isomers of $SiOH^+$–Ar have to be considered, as they have comparable binding energies and vibrational frequencies. Complexes of Ar with $OSiH^+$ may also be produced in the ion source, but they are not expected to have strong IR transitions in the investigated frequency range [45,47,48]. The spectroscopic and isomeric assignments indicated in Fig. 3 are based on the positions, intensities and rotational structure of the observed bands, and the comparison with the results of the ab initio calculations.

The most intense band with origin at 3444.9 cm^{-1} is assigned to the ν_1 fundamental of the linear proton-bound $SiOH^+$–Ar isomer. The Σ–Σ type character of this band, as well as the substantial red shift with respect to the monomer ν_1 frequency supports this interpretation. The experimental ν_1 shift of 217 cm^{-1} agrees well with the calculated shift of 246 cm^{-1}. Moreover, a similar complexation induced red shift of 274 cm^{-1} has previously been measured for the C–H frequency of the related linear proton-bound Ar–HCO^+ ionic complex [22]. On the other hand, for the anti-linear and T-shaped isomers of $SiOH^+$–Ar only small ν_1 shifts are calculated (Table 2).

The rotational analysis of the other two resolved bands at 3554.6 and 3581.5 cm^{-1} shows that they originate from the same vibrational level as the strong transition assigned to the ν_1 fundamental of the proton-bound dimer. As the linear $SiOH^+$–Ar isomer is not expected to have intense intramolecular overtones or combination bands [44], the two Σ–Σ type transitions appearing 109.6 and 136.6 cm^{-1} to the blue of ν_1 are attributed to combination bands of ν_1 with intermolecular vibrations. The ab initio calculation predicts scaled harmonic frequencies of $\nu_s = 116$ cm^{-1} and $\nu_b = 84$ cm^{-1} for the ground state of the linear isomer. Consequently, the lower energy band can be associated with $\nu_1 + \nu_s$ while the higher lying transition is interpreted as the $l = 0$ component of the $\nu_1 + 2\nu_b$ combination band. The latter assignment is somewhat tentative in view of the fact that the $\nu_1 + \nu_b$ combination (expected to be stronger than $\nu_1 + 2\nu_b$) has not been observed. However, the $\nu_1 + 2\nu_b$ transition (as well as other possible combinations of intra- and intermolecular vibrations) may acquire intensity from a Fermi-type interaction with the close lying $\nu_1 + \nu_s$ state. The $\nu_1 + 2\nu_b$ assignment is favored at this stage as it is compatible with the rotational structure and vibrational position anticipated for this band (see below). A simple deperturbation analysis was conducted assuming that the $\nu_1 + 2\nu_b$ band borrows all its intensity from the $\nu_1 + \nu_s$ state [64]. From the intensity ratio (3.5 ± 1.0) and the relative spacing (26.95 cm^{-1}) of the two bands an interaction parameter of 11.3 ± 0.9 cm^{-1} and a zero-order splitting of 14.4 ± 2.8 cm^{-1} could be derived. This yields deperturbed frequencies of 115.9 ± 1.4 and 130.3 ± 1.4 cm^{-1} for the ν_s and $2\nu_b$ modes in the ν_1 state, respectively.

The unresolved feature at 3673 ± 5 cm^{-1} is significantly broader (fwhm ≈ 25 cm^{-1}) than all other observed bands and appears with significant intensity ~ 230 cm^{-1} to the blue of the ν_1 transition of the proton-bound dimer. An assignment to the intramolecular combination band $\nu_1 + \nu_2$ of this isomer appears unlikely, as the monomer ν_2 frequency, estimated as 373 ± 10 cm^{-1} [46], is predicted to substantially increase upon complex formation. The position of the broad feature would be compatible with an assignment to the Fermi triad $\nu_1 + 2\nu_s$, $\nu_1 + \nu_s + 2\nu_b$ and $\nu_1 + 4\nu_b$; however, such an interpretation cannot account for the relatively large intensity of this band. Therefore, this transition is attributed to the ν_1 fundamental of the T-shaped isomer. The calculation predicts a complexation induced blue shift of $+16$ cm^{-1} for the ν_1 vibration of this isomer, in close agreement with the measured value of $+11 \pm 5$ cm^{-1}. Furthermore, the binding energy (D_e) of the T-shaped isomer is predicted to be only 16% lower than that of the proton-bound dimer, suggesting that both isomers might be produced with comparable abundances in the employed

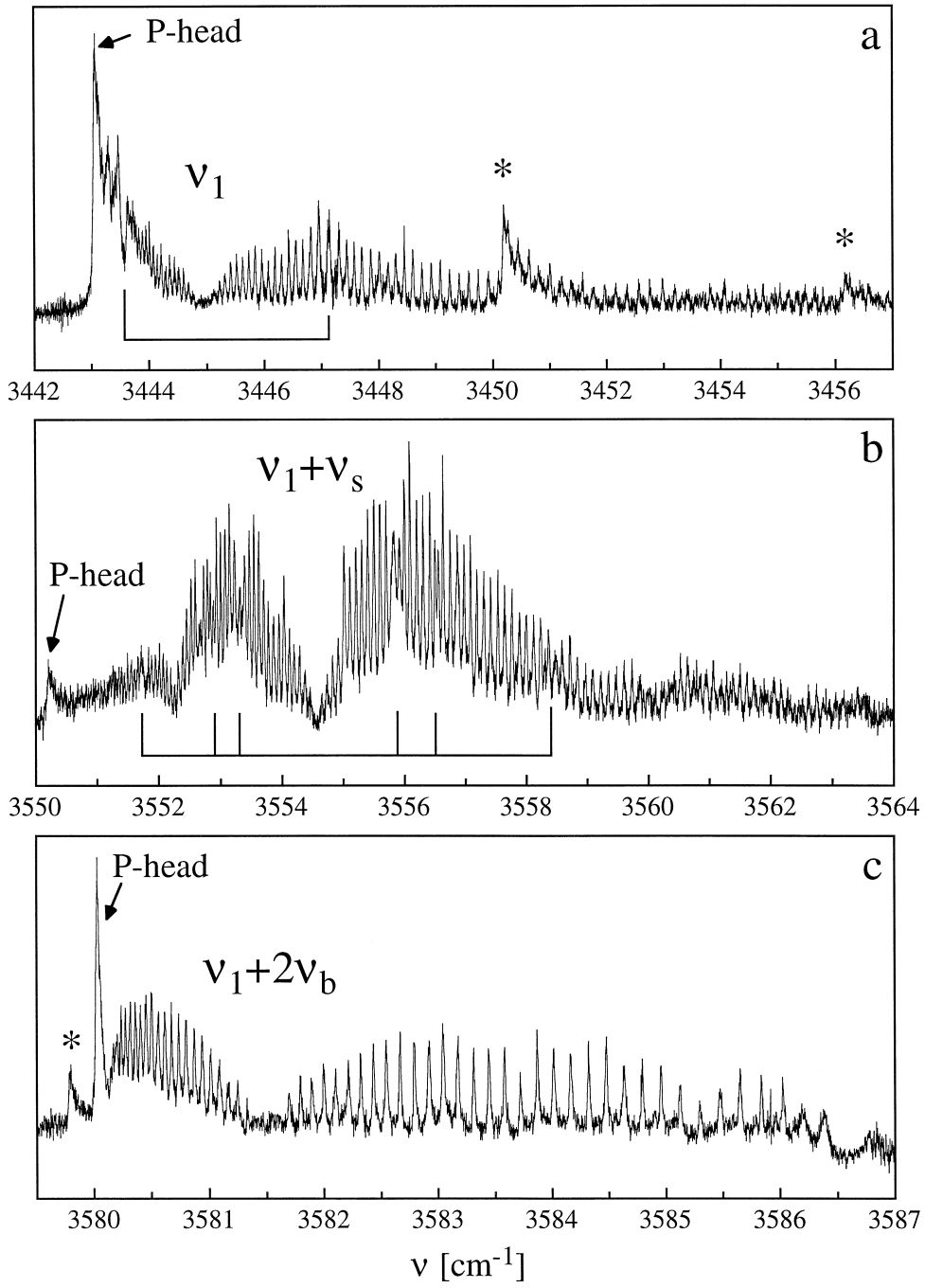

Fig. 4. Detailed view of the rotationally resolved transitions of the proton-bound linear $SiOH^+$–Ar dimer. The bars indicate the occurrence of strong perturbations. Peaks (heads) marked by asterisks are assigned to sequence transitions.

ion source. Using the integrated intensity ratio of the ν_1 bands of the linear and T-shaped isomers (~ 5–10) and the respective theoretical transition strengths from Table 2, the population ratio is estimated as 1.6–3.1 in favor of the linear isomer.

Due to the limited signal-to-noise ratio in the band gap region the rotational assignment of the resolved Σ–Σ transitions of the linear isomer was somewhat ambiguous (to ± 1 in J), except for the $\nu_1 + \nu_s$ band for which the R(0) and P(1) lines were clearly discernible. The rotational lines of the other two bands could be rigorously assigned by considering the lower state combination differences (CD) for the ν_1 and $\nu_1 + 2\nu_b$ bands, which were found to agree with those of the $\nu_1 + \nu_s$ band only for a single choice of J numbering. The agreement between the CD of all three rotationally-resolved bands supports their assignment to transitions originating from the same lower state, the vibrational ground state of the linear dimer. From a Boltzmann plot of the $\nu_1 + \nu_s$ band the rotational temperature of low J levels was estimated as 30 K, whereas higher J levels had a population corresponding to a much higher temperature of ~ 110 K. In agreement with previous observations [24,33] it was found that the efficiency of rotational cooling in the employed ion source decreases for levels with increasing rotational energy, leading to the observed non-thermal population distribution.

The molecular constants of the linear isomer were obtained by least-squares fitting of experimental CD and/or transition frequencies to a standard linear molecule Hamiltonian, $\hat{H} = \nu_0 + B\hat{J}^2 - D\hat{J}^4$. Table 3 summarizes the resulting parameters, the standard deviations and the lines used in the fits. The ground state molecular constants were determined from the CD ranging from $\Delta_2 F''(1)$ to $\Delta_2 F''(54)$ obtained by averaging the individual lower state CD of the three resolved bands. The constants of the ν_1, $\nu_1 + \nu_s$ and $\nu_1 + 2\nu_b$ vibrational states were obtained by fitting the respective measured transition frequencies while keeping the ground state constants fixed at the values obtained from the CD analysis. Several strong local perturbations were identified and the corresponding transitions were excluded from the fits. These include $J = 17$–20 of the ν_1 state and $J = 13$, 14, 19, 20, and 37 of the $\nu_1 + \nu_s$ state (Fig. 4). Similarly, the R branch lines of the $\nu_1 + 2\nu_b$ band terminating at $J' > 25$ were excluded from the final fit, as systematically increasing discrepancies between

Table 3
Molecular constants of several vibrational states of the linear proton-bound $SiOH^+$–Ar dimer and intermolecular distances derived from the rotational constants

	Ground state	ν_1	$\nu_1 + \nu_s$	$\nu_1 + 2\nu_b$
ν_0 (cm^{-1})[a]	–	3444.945(4)	3554.558(2)	3581.508(2)
$B \times 10^2$ (cm^{-1})	4.4737(24)	4.5803(19)	4.5178(45)	4.6104(65)
$D \times 10^8$ (cm^{-1})	3.2(6)	3.2[b]	3.5(1.1)	3.2[b]
assigned lines and CD[c]	$\Delta_2 F''(2$–$54)$	P(2–24) R(1–39)	P(1–55) R(0–53)	P(2–21) R(1–32)
excluded lines	–	P(18–21) R(16–19)	P(14, 15, 21, 38) R(12, 13, 19, 36)	R(25–32)
$\sigma \times 10^3$ (cm^{-1})	5.7	8.0	5.9	2.4
R_{cm} (Å)	4.062(1)	4.010(9)	4.040(2)	3.996(3)
r_{H-Ar} (Å)[d]	2.186(1)	2.134(9)	2.164(2)	2.120(3)

Also included are the observed rotational lines for each transition, the lines excluded from the fits and the respective standard deviations.
[a] Absolute precision of the calibration is 0.01 cm^{-1}.
[b] Fixed at ground state value.
[c] Calibrated line positions are available upon request.
[d] Determined from R_{cm} assuming an undistorted $SiOH^+$ geometry: $r_{Si-O} = 1.537$ Å and $r_{Si-O} = 0.940$ Å (Ref. [51]).

measured and calculated energies indicated a possible perturbation at higher J' levels.

Treating the $SiOH^+$–Ar complex as a pseudo-diatomic molecule [65], intermolecular center-of-mass separations $R_{cm} = \langle 1/R^2 \rangle^{-1/2}$, r_{H-Ar} distances, and harmonic force constants (k_s) and frequencies (ω_s) of the intermolecular stretching vibration can be derived from the measured rotational and centrifugal distortion constants under the assumption that the monomer is not distorted upon formation of the complex (Tables 3 and 4). The ab initio calculations suggest that the O–H separation increases by 0.011 Å on going from the monomer to the linear proton-bound dimer, and the values given in Table 3 may therefore be corrected by this amount to obtain better estimates for r_{H-Ar}.

For the ground vibrational state of the linear isomer, the intermolecular center-of-mass separation $R_{cm} = 4.06$ Å implies an interatomic bond length $r_{H-Ar} = 2.19$ Å (2.18 Å after the correction), in satisfying agreement with the ab initio values of $R_{cm} =$ 4.02 Å and $r_{H-Ar} = 2.10$ Å, respectively. Excitation of the OH stretch vibration leads to a significant stabilization of the intermolecular bond. This effect is evident from the red shift in the ν_1 frequency upon complexation and the contraction of the intermolecular bond upon ν_1 excitation by ~ 0.05 Å, giving rise to the P branch head at 3443.07 cm^{-1} ($J = 42$). Closer inspection of the spectrum in the blue wing of the ν_1 band reveals several weaker head-like features, the most intense ones being separated by 7.1 and 13.1 cm^{-1} from the ν_1 head (Fig. 4a). They are attributed to sequence transitions involving ν_1 and intermolecular modes. As the intermolecular interaction is stronger in the ν_1 excited state, the frequencies ν_s and ν_b should be larger compared to those in the $\nu_1 = 0$ state of $SiOH^+$–Ar. Thus, sequence transitions of the form $\nu_1 + n\nu_s + m\nu_b \leftarrow n\nu_s + m\nu_b$ should appear to the blue of ν_1 with decreasing intensities for increasing n and m. A tentative assignment of the strongest head at 3450.2 cm^{-1} to the P branch of $\nu_1 + \nu_s \leftarrow \nu_s$ transition yields an estimated ground state intermolecular stretch frequency of $\nu_s \approx 103$ cm^{-1}, in close agreement with the value obtained from the rotational analysis ($\omega_s = 102 \pm 10$ cm^{-1}).

The assignment of the transition at 3554.6 cm^{-1} to the $\nu_1 + \nu_s$ combination band of the linear isomer is consistent with the extracted molecular constants. In comparison to the ν_1 state the rotational constant decreases in the $\nu_1 + \nu_s$ state, reflecting the stretching of the averaged intermolecular bond by 0.03 Å upon excitation of ν_s. Consequently, the P branch head moves to higher J levels ($J > 75$). As the interaction increases upon ν_1 excitation, the intermolecular stretching frequency in the ν_1 state, $\nu_s =$ 109.6 cm^{-1} (115.9 cm^{-1} deperturbed), is also larger than the corresponding ground state value, $\nu_s \approx 103$ cm^{-1}. Excitation of $2\nu_b$ in the intramolecular ν_1 state shrinks the intermolecular bond by 0.014 Å. A slight bond contraction is indeed expected for the excitation of intermolecular bending vibration(s) in a linear rod-and-ball complex. The deduced frequency of $2\nu_b = 136.6$ cm^{-1} (130.3 cm^{-1} deperturbed) in the ν_1 state is significantly lower than the harmonic value of 168 cm^{-1} calculated for the ground state. Possible reasons for this discrepancy include different bending force constants in both intramolecular states, large anharmonicities in the bending coordinate, significant angular–radial couplings, an insufficient theoretical level, or an incorrect assignment. A weak feature observed 0.23 cm^{-1} to the red of the $\nu_1 + 2\nu_b$ head (Fig. 4c) is attributed to a sequence band of the type $\nu_1 + 2\nu_b + \nu_x \leftarrow \nu_x$, where ν_x is tentatively associated with ν_s.

The width of the rotational lines of all three transitions attributed to the linear $SiOH^+$–Ar structure is limited by the laser resolution of 0.02 cm^{-1}. Consequently, a lower limit for the respective upper state lifetimes (τ) of 250 ps can be derived. The

Table 4
Comparison of several properties of the intermolecular bond in linear proton-bound AH^+–Ar complexes

AH^+–Ar	$SiOH^+$–Ar	OCH^+–Ar	NNH^+–Ar
PA_A (kJ/mol)	792[b]	594[c]	495[c]
ΔPA_{A-Ar} (kJ/mol)[a]	421	223	124
D_e (cm^{-1})	1117	1619[d]	~ 3000[e]
$\Delta\nu_1$ (cm^{-1})	−217	−274[d]	< -700[e]
k_s (N/m)	13	17[d]	38[e]
r_{H-Ar} (Å)	2.19	2.13[d]	1.90[e]

[a] $PA_{Ar} = 371$ kJ/mol (Ref. [18]).
[b] Ref. [53].
[c] Ref. [18].
[d] Refs. [22,35,38].
[e] Refs. [27,60].

observation that the photodissociation process occurs on a time scale shorter than the flight time of the ions through the octopole provides an upper limit, $\tau < 50$ μs. Interestingly, no rotational substructure is discernible in the ν_1 band of the T-shaped isomer, although contour simulations assuming the ab initio structure ($A = 0.6447$ cm^{-1}, $B = 0.0770$ cm^{-1}, $C = 0.0688$ cm^{-1}) and a rotational temperature distribution similar to that of the linear dimer suggest that rotational resolution should be achievable with the employed laser. It is assumed that the apparent broadening results from spectral congestion due to a number of overlapping sequence transitions. In contrast to the linear isomer, the frequencies of the intermolecular vibrations of the T-shaped complex should be less sensitive to OH stretch excitation. Thus, sequence bands like $\nu_1 + \nu_s \leftarrow \nu_s$ (observed for the linear complex) all overlap with the ν_1 fundamental. Homogeneous line broadening due to short upper state lifetimes is not likely to contribute to the line width, as vibrational predissociation and/or energy redistribution is expected to be faster for the linear isomer due to the more efficient coupling between the OH stretch and dissociation coordinates. Finally, it is noted that the total width of the simulated ν_1 hybrid band of the T-shaped isomer is compatible with the observed one, adding some confidence to the assignment of the broad band to this particular isomer.

The structural, dynamic and energetic parameters of the proton-bound linear $SiOH^+$–Ar dimer may be compared with those of the N_2H^+–Ar and OCH^+–Ar dimers (Table 4). The intermolecular bond strength in AH^+–B type complexes is correlated with the difference in the proton affinities of the two bases A and B, $\Delta PA_{AB} = PA_A - PA_B$ [34]. As the proton affinities of SiO, CO and N_2 decrease in the row $PA_{SiO} > PA_{CO} > PA_{NN}$, the intermolecular interaction strength in complexes composed of their protonated ions with Ar increases in the same order. This trend is reflected in increasing binding energies, intermolecular stretching force constants and complexation induced ν_1 (i.e., AH stretch) red shifts as well as the decreasing H–Ar bond lengths (Table 4).

4.2. Larger complexes $SiOH^+$–Ar_n ($n = 2$–10)

Predissociation spectra of larger $SiOH^+$–Ar_n complexes with n up to 10 were recorded in the vicinity of the ν_1 vibration of the $SiOH^+$ chromophore (Fig. 5) and the observed band maxima with their assignments are summarized in Table 5. Though the transitions lack rotational structure, the observed systematic band shifts as a function of the cluster size provide valuable information on the cluster growth and the existence and stability of various coexisting isomers. Moreover, the analysis of the spectra of the larger clusters confirms the assignments for the transitions of the dimer presented in Section 4.1.

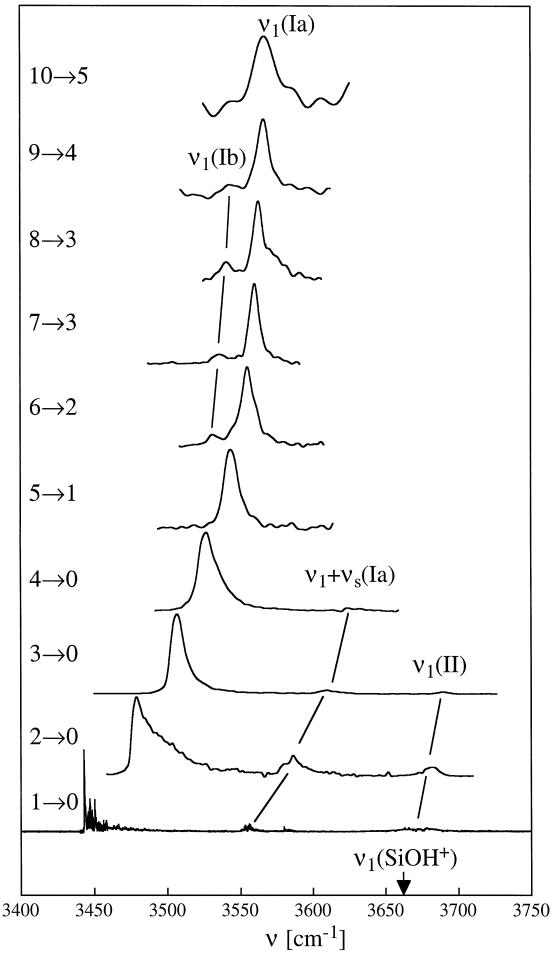

Fig. 5. Photofragmentation spectra of mass-selected $SiOH^+$–Ar_n complexes ($n = 1$–10) recorded in the respective dominant fragment $SiOH^+$–Ar_m channel (indicated as $n \rightarrow m$). The observed transitions are assigned to different isomeric forms (Ia, Ib, and II). Connecting lines show corresponding transitions.

Table 5
Measured band maxima[a] (in cm^{-1}) of $SiOH^+–Ar_n$ clusters

n	Isomer Ia		Isomer Ib	Isomer II
	ν_1 ($\Delta\nu_1$)	$\nu_1+\nu_s$ (ν_s)	ν_1 ($\Delta\nu_1$)	ν_1 ($\Delta\nu_1$)
1	3444.9[b] (−217)	3554.5[b] (109.6)		3673 (11)
2	3479 (−183)	3587 (108)		3681 (19)
3	3506 (−156)	3610 (104)		3690 (28)
4	3526 (−136)	3624 (98)		
5	3543 (−119)			
6	3555 (−107)		3531 (−131)	
7	3560 (−102)		3536 (−126)	
8	3563 (−99)		3541 (−121)	
9	3566 (−96)		3545 (−117)	
10	3567 (−95)			

[a]Uncertainty ± 1 cm^{-1}.
[b]Band origins ν_0.
The values in brackets present the total complexation induced ν_1 frequency shifts in ($\Delta\nu_1=\nu_1^{complex}-\nu_1^{monomer}$) or the frequency ν_s in the ν_1 state.

First, the frequency shifts of the most intense transition are considered (Figs. 5 and 6; Table 5). As outlined above, the band at 3445 cm^{-1} in the $SiOH^+$–Ar dimer spectrum is assigned to the ν_1 transition of the linear proton-bound complex (isomer I), based on the rotational analysis and the comparison with the ab initio data. The large complexation induced red shift of 217 cm^{-1} indicates that there is significant proton transfer from SiO to Ar, which destabilizes the intramolecular O–H bond. Addition of further Ar atoms shifts this band monotonically back to the blue, indicating that the O–H bond strength gains in stability again. The stabilization effect caused by adding one further Ar atom into the solvation shell becomes gradually smaller for increasing number of Ar ligands, as is evidenced by the decreasing incremental shifts, $\Delta\nu_1(n)=\nu_1(n)-\nu_1(n-1)$. They start at 34 cm^{-1} ($n=2$) and appear to converge to values below 1 cm^{-1} giving rise to an absolute blue shift of 95 cm^{-1} ($n=10$). Unfortunately, it appears that no Ar matrix isolation studies of $SiOH^+$ have been carried out, preventing a direct comparison of the band shifts with the bulk limit.

The band lying $\sim$100–110 cm^{-1} to higher frequency from ν_1 correlates with the $\nu_1+\nu_s$ transition of the linear $SiOH^+$–Ar dimer. A similar transition was observed in the spectra of the related $HCO^+–Ar_n$ series [22]. The occurrence of this band for clusters with $n>1$ may be interpreted as evidence that the first Ar atom in the $SiOH^+–Ar_n$ clusters remains at the proton-bound site. Considerably different intermolecular stretching frequencies are anticipated for alternative structures, e.g. a T-shaped geometry for the $SiOH^+–Ar_2$ trimer wherein the $SiOH^+$ moiety points towards the midpoint of an Ar dimer. The separation between the ν_1 and $\nu_1+\nu_s$ band maxima decreases with increasing cluster size, suggesting an anti-correlation between the O–H and H–Ar bond stabilities.

The most conceivable cluster geometries (denoted isomer series Ia) responsible for the transitions mentioned above are those where Ar atoms with $n\geq 2$ surround a linear $SiOH^+$–Ar core. As the T-shaped Si-bound configuration of the $SiOH^+$–Ar dimer is predicted to be a deep (local) minimum, subsequent Ar atoms may occupy positions in a solvation ring around the $SiOH^+$–Ar rod near the Si atom. Filling this ring may result in a monotonic change of the charge distribution on the chromophore ion which sensitively influences the intermolecular bond strength to the first Ar atom. As the number of ligands increases this intermolecular bond becomes weaker, which in turn strengthens the intramolecular O–H bond. Consequently, the ν_1 frequency increases, while at the same time the frequency of the intermolecular H–Ar stretch of the first Ar atom (ν_s) gradually decreases, in agreement with the experimental observation (Table 5). After the first solvation ring is filled (with 4–5 Ar atoms), additional Ar atoms may occupy positions in a second ring centered around the O–H bond.

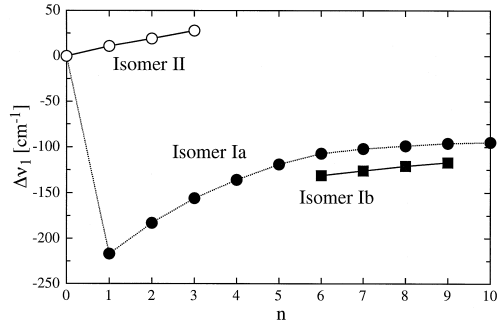

Fig. 6. Complexation induced frequency shift of the ν_1 vibration of the different isomeric structures of $SiOH^+–Ar_n$ complexes as a function of the cluster size.

Interestingly, in the size range $n = 6$–9 a weak satellite appears to the red of the ν_1 band of each cluster. This bifurcation starts at $n = 6$, i.e. approximately at the cluster size where the first solvation ring around the linear proton-bound dimer core is closed and the second ring is starting to be filled. This bifurcation is interpreted as coexistence of two isomeric structures for each cluster size with $n \geq 6$ (denoted Ia and Ib, respectively), one having 5 and the other having 4 Ar atoms in the first solvation ring. From the large difference in the relative intensities of the two bands one may conclude that the stability and therefore the abundance of both isomers, are quite different.

Apart from the bands assigned to isomers possessing a proton-bound dimer core (Ia and Ib), the spectra of the complexes with $n = 1$–3 show weak bands shifted slightly to the blue of the $SiOH^+$ ν_1 band (Figs. 5 and 6). The total shift in the band positions increases linearly with cluster size with a rate of $\sim 10\ cm^{-1}$ per Ar atom. In Section 4.1 the corresponding $SiOH^+$–Ar dimer band was attributed to the ν_1 transition of the T-shaped structure (isomer II) based on the ab initio calculation. Equidistant incremental band shifts for increasing cluster size usually imply the occupation of isostructural positions within the solvation shell. Thus, the observed bands in the trimer and tetramer spectra are attributed to structures with respectively two and three Ar atoms in a solvation ring around the Si atom of the $SiOH^+$ monomer, i.e. geometries *without* a proton-bound Ar ligand.

The spectra of the $SiOH^+$–Ar_n series may be compared with those of the related HCO^+–Ar_n series [22]. As the proton-bound structure is the only minimum on the Ar–HCO^+ dimer surface, all spectral features of the $SiOH^+$–Ar_n series arising from isomer II have no analogue in the case of HCO^+–Ar_n. On the contrary the features arising from isomers Ia and Ib are quite similar in both cases. The linear proton-bound Ar–HCO^+ dimer features a large ν_1 (CH stretch) red shift upon complexation, further Ar atoms shift the transition monotonically back to the blue, and the bifurcation also occurs at $n = 6$. However, the spectral signatures for the formation of the two solvation rings are more prominent for HCO^+–Ar_n, as in this case the bands arising from isomer Ib are much more intense than those of isomer Ia. In fact, in the previous study on HCO^+–Ar_n the much weaker higher frequency bands were not recognized as arising from a second isomer, but they were tentatively attributed to a combination band of ν_1 with a low-frequency intermolecular mode of a single isomer [22]. However, as for $SiOH^+$–Ar_n the higher energy band is much more intense, it cannot be attributed to a combination band, and therefore the model with the coexistence of two isomers (Ia, Ib) in both $SiOH^+$–Ar_n and HCO^+–Ar_n complexes for $n \geq 6$ is presently favored.

The photon energy deposited in the $SiOH^+$–Ar_n complexes is sufficient for evaporating a few Ar atoms. Consequently, several fragment channels $SiOH^+$–Ar_m ($m < n$) are possible following absorption, and they were examined for excitation at the ν_1 maxima of the Ia isomers. Similarly to previous studies on HCO^+–Ar_n ($n = 1$–13 [22]) and NH_3^+–Ar_n ($n = 1$–7 [31]) complexes, a very narrow range of fragment channels has been observed for each parent cluster size (Table 6). Only for $n = 4$ and 8 more than one significant fragment channel ($> 5\%$) was found. The spectra were recorded for each of them and were observed to be very similar. Clusters with $n < 4$ lose all ligands, while from $n = 4$ to $n = 10$ the averaged number of Ar atoms lost ($\langle n - m \rangle$) increases monotonically from four to five.

From the absorbed photon energy ($\sim 3500\ cm^{-1}$) and the cluster size dependent number of evaporated Ar ligands, the incremental binding energies, $\Delta D_0(n) = D_0(n) - D_0(n-1)$, can be estimated based on the following approximations. First, the kinetic energy release as well as the differences in the internal energies of the parent and respective daughter clusters are neglected. Second, Ar atoms

Table 6
Photofragmentation ratios of $SiOH^+$–Ar_n complexes for excitation at the ν_1 band maxima of isomer Ia and fragmentation into $SiOH^+$–Ar_m and $(n - m)$ Ar atoms

n	1	2	3	4	5	6	7	8	9	10
m	0	0	0	0 (0.29) 1 (0.63) 2 (0.08)	1	2	3	3 (0.67) 4 (0.33)	4	5
$\langle n - m \rangle$	1	2	3	3.21	4	4	4	4.67	5	5

Only channels contributing more than 5% are listed. Uncertainties are estimated as 0.05.

situated at equivalent positions within the cluster are assumed to have the same binding energy. This yields (averaged) binding energies of 875 cm^{-1} < $\Delta D_0(1)$ < 1400 cm^{-1} for the proton-bound Ar atom, 700 cm^{-1} < $\Delta D_0(2–6)$ < 875 cm^{-1} for the 5 Ar atoms in the first solvation ring, and 440 cm^{-1} < $\Delta D_0(7–12)$ < 700 cm^{-1} for further 5 Ar atoms in the second ring. These values correlate with ab initio dimer binding energies, where the Ar atom is situated at the linear proton-bound configuration (D_e = 1117 cm^{-1}), the T-shaped minimum (D_e = 938 cm^{-1}), and an intermediate position ($D_e \approx 450$ cm^{-1}). Though zero-point effects and three-body interactions may to some extent influence the values for the individual incremental binding energies, the semi-quantitative agreement between the values obtained from the fragmentation ratios and the dimer ab initio potential surface supports the simple microsolvation model developed above for the isomer series Ia and Ib, where the first Ar atom occupies the proton-bound site and further Ar ligands fill two 4–5 membered equatorial solvation rings around the Si atom and the OH bond, respectively.

5. Conclusions

The intermolecular interaction in $SiOH^+–Ar_n$ complexes has been studied by means of IR photodissociation spectroscopy (n = 1–10) and ab initio methods (n = 1). Both the rotationally resolved IR spectrum and the calculations show that the global minimum on the potential energy surface of the $SiOH^+$–Ar dimer corresponds to a linear proton-bound structure with an intermolecular center-of-mass separation $R_{cm} = 4.06$ Å and a binding energy $D_e \approx 1100$ cm^{-1}. Complexation at the proton end of $SiOH^+$ leads to a significant red shift of the ν_1 (O–H stretch) vibration, $\Delta\nu_1 = -217$ cm^{-1}. The calculations predict a second, slightly less stable T-shaped isomer with the Ar ligand close to the Si atom of $SiOH^+$ ($D_e \approx 950$ cm^{-1}) and the experimental spectrum supports the existence of such an isomer by showing a broad band only slightly blue-shifted from the monomer ν_1 fundamental. Comparison of the properties of the proton-bound $SiOH^+$–Ar dimer with those of the related OCH^+–Ar and N_2H^+–Ar complexes provides spectroscopic evidence that the intermolecular bond strengths in proton-bound complexes of the type AH^+–B are correlated to the differences in the proton affinities of the two bases A and B. As induction interactions dominate the attractive part of the intermolecular potential in complexes of ions with rare gas atoms, the differing charge distributions in the ionic chromophores cause noticeable differences in the topologies of the respective dimer surfaces. For example, though all three of the above-mentioned complexes have a proton-bound global minimum, only for $SiOH^+$–Ar evidence for the existence of a stable T-shaped structure has been found. The formation of larger polymers depends also sensitively on the charge distribution, as evidenced by the different cluster growth mechanisms deduced from the systematic vibrational band shifts in the larger clusters' spectra as a function of their size. In the case of $SiOH^+–Ar_n$ the most stable isomers possess geometries, where the first Ar occupies a privileged proton-bound site and subsequent ligands fill two five-membered equatorial solvation rings around the Si atom (first ring) and the OH bond (second ring).

Acknowledgements

This study is part of the project No. 20-49104.96 of the Swiss National Science Foundation.

References

[1] J.O. Hirschfelder, C.F. Curtis, R.B. Bird, Molecular Theory of Gases and Liquids, Wiley, New York, 1954.
[2] P. Hobza, R. Zahradnik, Intermolecular Complexes: The Role of van der Waals Systems in Physical Chemistry and in the Biodisciplines, Elsevier, Amsterdam, 1988.
[3] S.N. Vinograd, R.H. Linnell, Hydrogen Bonding, Van Nostrand, New York, 1971.
[4] K.R. Leopold, G.T. Fraser, S.E. Novick, W. Klemperer, Chem. Rev. 94 (1994) 1807.
[5] A. van der Avoird, P.E.S. Wormer, R. Moszynski, Chem. Rev. 94 (1994) 1931.
[6] D.J. Nesbitt, Annu. Rev. Phys. Chem. 45 (1994) 367.
[7] J.M. Hutson, J. Chem. Phys. 96 (1992) 6752.
[8] M.J. Elrod, R.J. Saykally, Chem. Rev. 94 (1994) 1975.
[9] E.J. Bieske, J.P. Maier, Chem. Rev. 93 (1993) 2603.
[10] M. Okumura, L.I. Yeh, Y.T. Lee, J. Chem. Phys. 83 (1985) 3705.

[11] A. Carrington, D.I. Gammie, A.M. Shaw, S.M. Taylor, J.M. Hutson, Chem. Phys. Lett. 260 (1996) 395.
[12] M.W. Crofton, J.M. Price, Y.T. Lee, in: H. Haberland (Ed.), Clusters of Atoms and Molecules II, vol. 56, Springer, Berlin, 1994.
[13] J.M. Lisy, in: C.-Y. Ng, T. Baer, I. Powis (Eds.), Cluster Ions, Wiley, New York, 1993.
[14] M.A. Duncan, Annu. Rev. Phys. Chem. 48 (1997) 69.
[15] E.J. Bieske, J. Chem. Soc., Faraday Trans. 91 (1995) 1.
[16] P.B. Armentrout, T. Baer, J. Phys. Chem. 100 (1996) 12866.
[17] D. Smith, Chem. Rev. 92 (1992) 1473.
[18] S.G. Lias, J.E. Barmess, J.F. Liebman, J.L. Holmes, R.D. Levin, W.G. Mallard, J. Phys. Chem. Ref. Data Suppl. 17 (1988) 1.
[19] C. Lifshitz, in: C.-Y. Ng, T. Baer, I. Powis, Cluster Ions, Wiley, New York, 1993.
[20] S.A. Nizkorodov, J.P. Maier, E.J. Bieske, J. Chem. Phys. 103 (1995) 1297.
[21] S.A. Nizkorodov, O. Dopfer, M. Meuwly, J.P. Maier, E.J. Bieske, J. Chem. Phys. 105 (1996) 1770.
[22] S.A. Nizkorodov, O. Dopfer, T. Ruchti, M. Meuwly, J.P. Maier, E.J. Bieske, J. Phys. Chem. 99 (1995) 17118.
[23] E.J. Bieske, S.A. Nizkorodov, F.R. Bennett, J.P. Maier, J. Chem. Phys. 102 (1995) 5152.
[24] R.V. Olkhov, S.A. Nizkorodov, O. Dopfer, J. Chem. Phys. 107 (1997) 8229.
[25] S.A. Nizkorodov, J.P. Maier, E.J. Bieske, J. Chem. Phys. 102 (1995) 5570.
[26] S.A. Nizkorodov, M. Meuwly, J.P. Maier, O. Dopfer, E.J. Bieske, J. Chem. Phys. 108 (1998) 8964.
[27] S.A. Nizkorodov, Y. Spinelli, E.J. Bieske, J.P. Maier, O. Dopfer, Chem. Phys. Lett. 265 (1997) 303.
[28] E.J. Bieske, S.A. Nizkorodov, F. Bennett, J.P. Maier, Int. J. Mass Spectrom. Ion Process. 150 (1995) 167.
[29] O. Dopfer, S.A. Nizkorodov, M. Meuwly, E.J. Bieske, J.P. Maier, Chem. Phys. Lett. 260 (1996) 545.
[30] E.J. Bieske, S.A. Nizkorodov, O. Dopfer, J.P. Maier, R.J. Stickland, B.J. Cotterell, B.J. Howard, Chem. Phys. Lett. 250 (1996) 266.
[31] O. Dopfer, S.A. Nizkorodov, M. Meuwly, E.J. Bieske, J.P. Maier, Int. J. Mass Spectrom. Ion Process. 167,168 (1997) 637.
[32] S.A. Nizkorodov, D. Roth, R.V. Olkhov, J.P. Maier, O. Dopfer, Chem. Phys. Lett. 278 (1997) 26.
[33] D. Roth, S.A. Nizkorodov, J.P. Maier, O. Dopfer, J. Chem. Phys. (1998, in press).
[34] M. Meot-Ner, J. Am. Chem. Soc. 106 (1984) 1257.
[35] Y. Ohshima, Y. Sumiyoshi, Y. Endo, J. Chem. Phys. 106 (1997) 2977.
[36] M. Meuwly, S.A. Nizkorodov, J.P. Maier, E.J. Bieske, J. Chem. Phys. 104 (1996) 3876.
[37] T. Speck, H. Linnartz, J.P. Maier, J. Chem. Phys. 107 (1997) 8706.
[38] M. Meuwly, S.A. Nizkorodov, E.J. Bieske, J.P. Maier, O. Dopfer, unpublished results (1998).
[39] R.V. Olkhov, S.A. Nizkorodov, O. Dopfer, J. Chem. Phys. 108 (1998) 10046.
[40] K. Hiraoka, I. Kudaka, S. Yamabe, Chem. Phys. Lett. 178 (1991) 103.
[41] T.J. Millar, Astrophys. Space Sci. 72 (1980) 509.
[42] J.L. Turner, A. Dalgarno, Astrophys. J. 213 (1977) 386.
[43] Y. Tao, Chem. Phys. Lett. 154 (1989) 374.
[44] P. Botschwina, P. Rosmus, J. Chem. Phys. 82 (1985) 1420.
[45] R. Srinivas, D. Sülzle, W. Koch, C.H. DePuy, H. Schwarz, J. Am. Chem. Soc. 113 (1991) 5970.
[46] P. Botschwina, M. Oswald, P. Sebald, J. Mol. Spectrosc. 155 (1992) 360.
[47] H.C. Tandon, N.K. Ray, J. Mol. Struct. (Theochem) 367 (1996) 62.
[48] Y. Yamaguchi, H.F. Schaefer III, J. Chem. Phys. 102 (1995) 5327.
[49] T.B. McMahon, P. Kebarle, J. Chem. Phys. 83 (1985) 3919.
[50] A. Fox, S. Wlodek, A.C. Hopkinson, M.H. Lien, M. Sylvain, C. Rodriquez, D.K. Bohme, J. Phys. Chem. 93 (1989) 1549.
[51] H.E. Warner, A. Fox, T. Amano, D.K. Bohme, J. Chem. Phys. 91 (1989) 5310.
[52] N. Moazzen-Ahmadi, A.R.W. McKellar, H.E. Warner, T. Amano, J. Chem. Phys. 91 (1989) 5313.
[53] S. Wlodek, A. Fox, D.K. Bohme, J. Am. Chem. Soc. 109 (1987) 6663.
[54] N.R. Daly, Rev. Sci. Instrum. 31 (1960) 264.
[55] G. Guelachvili, K.N. Rao, Handbook of Infrared Standards, Academic Press, London, 1993.
[56] M.J. Frisch, G.W. Trucks, H.B. Schlegel, P.M.W. Gill, B.G. Johnson, M.A. Robb, J.R. Cheeseman, T. Keith, G.A. Petersson, J.A. Montgomery, K. Raghavachari, M.A. Al-Laham, V.G. Zakrzewski, J.V. Ortiz, J.B. Foresman, J. Cioslowski, B.B. Stefanov, A. Nanayakkara, M. Challacombe, C.Y. Peng, P.Y. Ayala, W. Chen, M.W. Wong, J.L. Andres, E.S. Replogle, R. Gomperts, R.L. Martin, D.J. Fox, J.S. Binkley, D.J. Defrees, J. Baker, J.P. Stewart, M. Head-Gordon, C. Gonzales, J.A. Pople, Gaussian 94, Gaussian, Inc., Pittsburgh, PA, 1995.
[57] Extensible Computational Chemistry Environmental Basis Set Data Base, Version 10 (1996).
[58] S.F. Boys, F. Bernardi, Mol. Phys. 19 (1970) 553.
[59] G. Chalasinski, M.M. Szczesniak, Chem. Rev. 94 (1994) 1.
[60] M. Kolbuszewski, Chem. Phys. Lett. 244 (1995) 39.
[61] A. Nowek, J. Leszczynski, J. Chem. Phys. 105 (1996) 6388.
[62] A. Cunje, C.F. Rodriquez, D.K. Bohme, A.C. Hopkinson, J. Phys. Chem. A 102 (1998) 478.
[63] B. Weis, K. Yamashita, J. Chem. Phys. 99 (1993) 9512.
[64] C.H. Townes, A.L. Schawlow, Microwave Spectroscopy, Dover, New York, 1975.
[65] D.J. Millen, Can. J. Chem. 63 (1985) 1477.